A Quadratic Eigenvalue Solver of Linear Complexity for 3-D Electromagnetics-Based Analysis of Large-Scale Integrated Circuits

Jongwon Lee, *Student Member, IEEE,* Duo Chen, Venkataramanan Balakrishnan, *Senior Member, IEEE,* Cheng-Kok Koh, *Senior Member, IEEE,* and Dan Jiao, *Senior Member, IEEE*

***Abstract*—It is of critical importance to efficiently and accurately predict global resonances of a 3-D integrated circuit system that involves arbitrarily shaped lossy conductors and inhomogeneous materials. A quadratic eigenvalue solver of linear complexity and electromagnetic accuracy is developed in this paper to fulfill this task. Without sacrificing accuracy, the proposed eigenvalue solver has shown a clear advantage over state-of-the-art eigenvalue solvers in fast CPU time. It successfully solves a quadratic eigenvalue problem of over 2.5 million unknowns associated with a large-scale 3-D on-chip circuit embedded in inhomogeneous materials in 40 min on a single 3 GHz 8222SE AMD Opteron processor.**

***Index Terms*—Arnoldi iteration, fast solvers, finite element methods, full-wave analysis, integrated circuits, quadratic eigenvalue problem, resonance analysis.**

I. Introduction

INTEGRATION minimizes size and weight, and maximizes performance of circuits. However, integrating as many circuits as possible on the same chip leads often to undesired coupling and sometimes to system failure. For instance, switching currents induced by logic circuits cause ringing in the power-supply rails and in the output driver circuitry. This in turn couples through the common substrate to corrupt sensitive analog signals on the same chip. Prevailing circuit-based signal integrity paradigms are reaching their limits of predictive accuracy when applied to high-frequency mixed-signal settings. To sustain the scaling and integration of digital, analog, mixed-signal, and radio frequency (RF) circuitry, an electromagnetic solution is indispensable. Such a solution allows for an accurate characterization of analog/RF circuitry, their mutual coupling, their interaction with drivers/receivers, and their coupling to interconnects and substrate.

Manuscript received April 28, 2011; revised August 4, 2011; accepted September 11, 2011. Date of current version February 17, 2012. This work was supported in part by the National Science Foundation, under Awards 0747578 and 0702567, and in part by a grant from Intel Corporation. This paper was recommended by Associate Editor L. M. Silveira.

Jongwon Lee is with the Agency for Defense Development, Daejeon 305-600, Korea (e-mail: lee514@purdue.edu).

D. Chen, V. Balakrishnan, C.-K. Koh, and D. Jiao are with the School of Electrical and Computer Engineering, Purdue University, West Lafayette, IN 47907 USA (e-mail: chen256@purdue.edu; ragu@purdue.edu; chengkok@purdue.edu; djiao@purdue.edu).

Color versions of one or more of the figures in this paper are available online at http://ieeexplore.ieee.org.

Digital Object Identifier 10.1109/TCAD.2011.2170989

One of the critical needs in high-frequency integrated circuit (IC) design is to predict the resonance frequency of an integrated system. Although a chip design and its package design can each meet design targets, the actual packaged chip often fails at certain frequencies because of the resonance caused by the coupling between the die and the package. Therefore, it is important to accurately predict the resonance frequency of an integrated system for its removal. The resonance frequency of an IC system can be accurately found by solving a 3-D electromagnetics-based quadratic eigenvalue problem. The quadratic eigenvalue problem can be converted to a generalized eigenvalue problem via linearization. For solving a generalized eigenvalue problem of size N, the computational complexity of traditional eigenvalue solvers such as QR is $O(N^3)$. With state-of-the-art Arnoldi algorithms [5], [10], the complexity is reduced to $O(N^2)$. However, such a complexity is still inadequate for analyzing global resonances of an IC system since N is too large. When resonance occurs, the entire integrated system is excited. As a result, the number of unknowns, N, involved in the analysis of global resonances of an IC system is ultra large. In [2] and [3], the $O(N^2)$ complexity of an Arnoldi-based eigenvalue solution is reduced to $O(N)$ complexity for a 2.5-D finite-element based solution of Manhattan-type large-scale on-chip interconnects. In this solution, a 2-D generalized eigenvalue problem is formulated with the third dimension handled by mode matching technique. The eigenvalues found are complex propagation constants of the waves propagating in each 2-D structure seed. However, the IC structures that can be analyzed by a 2.5-D based solution are limited. For general problems encountered in the design of ICs such as arbitrarily shaped RF devices, high bandwidth package interconnects, and a combined die-package system, a 3-D solution is unavoidable. Since the linear-complexity complex-valued eigenvalue solvers in [2] and [3] were developed in the framework of a 2.5-D finite element-based formulation, the problem of finding a linear-complexity solution to the generalized eigenvalue problem remains open for the 3-D electromagnetics-based analysis of IC structures. If such a solution can be found, one can quickly obtain the complex resonance frequencies of the entire IC structure, which are nothing but the eigenvalues of the underlying 3-D quadratic eigenvalue problem, as well as the fundamental 3-D modes (field distributions)

that can be supported by the structure, which are eigenvectors.

The main contribution of this paper is the development of an eigenvalue solver of linear complexity for 3-D electromagnetics-based analysis of general IC structures. In this solver, a quadratic eigenvalue problem is first formulated for analyzing 3-D IC structures that involve arbitrarily shaped lossy conductors and nonuniform materials. The quadratic eigenvalue problem is then converted to a generalized eigenvalue problem to facilitate efficient computation. The computational bottleneck of the generalized eigenvalue problem is analyzed and found to be the solution of a large-scale 3-D sparse matrix. An orthogonal finite-element reduction-recovery method [4] is then employed to achieve a linear-complexity solution of the large-scale sparse matrix, holding the complexity of the entire eigenvalue solution to linear. Furthermore, the spurious eigenvalues associated with the orthogonal vector basis-based discretization of the generalized eigenvalue problem are identified. The origin of the spurious eigenvalues is analyzed, and the approach to removing the spurious eigenvalues is given. In addition, the accuracy of a quadratic eigenvalue solution is investigated. The backward error is introduced to quantitatively measure the accuracy of the proposed eigenvalue solution. An optimal scaling technique is used to transform the original quadratic eigenvalue problem to a scaled quadratic eigenvalue problem, improving the accuracy of the quadratic eigenvalue solution by a few orders of magnitude.

This paper is organized as follows. In Section II, we give a quadratic eigenvalue-based formulation for analyzing general 3-D IC problems involving lossy conductors and inhomogeneous materials. In Section III, we present a linear-complexity solution to the quadratic eigenvalue problem, analyze the spurious eigenvalues, investigate the accuracy of the quadratic eigenvalue solution, and present a scaled quadratic eigenvalue problem that significantly improves accuracy. In Section IV, numerical results are given to demonstrate the performance of the proposed solver. Section V relates to our conclusions.

II. Quadratic Eigenvalue Problem for 3-D Electromagnetics-Based Analysis of ICs

Inside a 3-D IC, the electric field $\mathbf{E}$ satisfies the following second-order vector wave equation:

$$\nabla \times \left(\frac{1}{\mu}\nabla \times \mathbf{E}\right) - (2\pi f_0)^2\,\varepsilon\mathbf{E} + j2\pi f_0\sigma\mathbf{E} = 0 \qquad (1)$$

where f_0 is frequency, μ, ε, and σ denote permeability, permittivity, and conductivity, respectively. Both dielectric and conductor loss can contribute to the term associated with conductivity. It is also worth mentioning that for on-chip and package circuits, conductors cannot be treated as perfect conductors because skin depth is comparable to the physical dimensions of conductors.

A finite element-based analysis [7] of (1) subject to its boundary conditions results in the following quadratic eigenvalue problem:

$$\left[\mathbf{S} + \lambda^2\mathbf{T} + \lambda\mathbf{R}\right]\{e\} = 0 \qquad (\lambda = jk_0) \qquad (2)$$

in which the eigenvalues λ correspond to complex resonant frequencies, and the eigenvectors e characterize the electric field at each edge in the computational domain. The $\mathbf{S}$, $\mathbf{T}$, and $\mathbf{R}$ are all real-valued matrices. Their elements are given by

$$\begin{aligned}\mathbf{S}_{ij} &= \iiint_V \frac{1}{\mu_r}\{\nabla \times \mathbf{N}_i\}\cdot\{\nabla \times \mathbf{N}_j\}dV\\ \mathbf{T}_{ij} &= \iiint_V \mu_0\varepsilon\mathbf{N}_i\cdot\mathbf{N}_j dV\\ \mathbf{R}_{ij} &= \iiint_V \mu_0\sigma\mathbf{N}_i\cdot\mathbf{N}_j dV\end{aligned} \qquad (3)$$

where $\mathbf{N}$ denotes the edge basis function used to expand the unknown electric field $\mathbf{E}$ in each element, and V is the computational domain. The quadratic eigenvalue problem shown in (2) can be solved by computing the roots of the determinant of the polynomial matrix

$$\mathbf{P}(\lambda) = \mathbf{S} + \lambda^2\mathbf{T} + \lambda\mathbf{R}. \qquad (4)$$

However, this scheme can be computationally expensive. To facilitate efficient computation of (2), we linearize the above quadratic eigenvalue problem to a generalized eigenvalue problem of twice the dimension

$$\begin{bmatrix} -\mathbf{S} & 0 \\ 0 & \mathbf{T}\end{bmatrix}\begin{Bmatrix} e \\ \lambda e\end{Bmatrix} = \lambda\begin{bmatrix}\mathbf{R} & \mathbf{T} \\ \mathbf{T} & 0\end{bmatrix}\begin{Bmatrix} e \\ \lambda e\end{Bmatrix} \qquad (5)$$

the solution of which is theoretically the same as that of (2).

Equation (5) can be compactly written as

$$\mathbf{A}'x = \lambda\mathbf{B}'x \qquad (6)$$

where $\mathbf{A}'$, $\mathbf{B}'$, and x are

$$\mathbf{A}' = \begin{bmatrix} -\mathbf{S} & 0 \\ 0 & \mathbf{T}\end{bmatrix}, \quad \mathbf{B}' = \begin{bmatrix}\mathbf{R} & \mathbf{T} \\ \mathbf{T} & 0\end{bmatrix}, \quad x = \begin{Bmatrix} e \\ \lambda e\end{Bmatrix}.$$

In many IC applications, we have to find only k selected eigenpairs of (6). For example, we are interested in a few lowest resonant frequencies of an IC, or the first k modes that are the closest to a frequency of interest. The Arnoldi iteration [10] is particularly suited for this computing task. The time and storage complexity of the Arnoldi iteration for solving (6) is at least quadratic due to the fact that $\mathbf{B}'^{-1}$ is generally dense. In the next section, we propose a linear-complexity solution of (6).

III. Proposed Linear-Complexity 3-D Eigenvalue Solution

This section includes a linear-complexity solution of (6), the identification of the spurious eigenvalues of (6) and its removal, and a scaled quadratic eigenvalue problem with optimal scaling for achieving good accuracy in eigenvalues and eigenvectors.

A. Linear-Complexity Solution

1) *Converting the Solution of a Generalized Eigenvalue Problem to the Solution of a Matrix:* In this section, we analyze the computational bottleneck of an Arnoldi-based solution of a generalized eigenvalue problem. We show that the

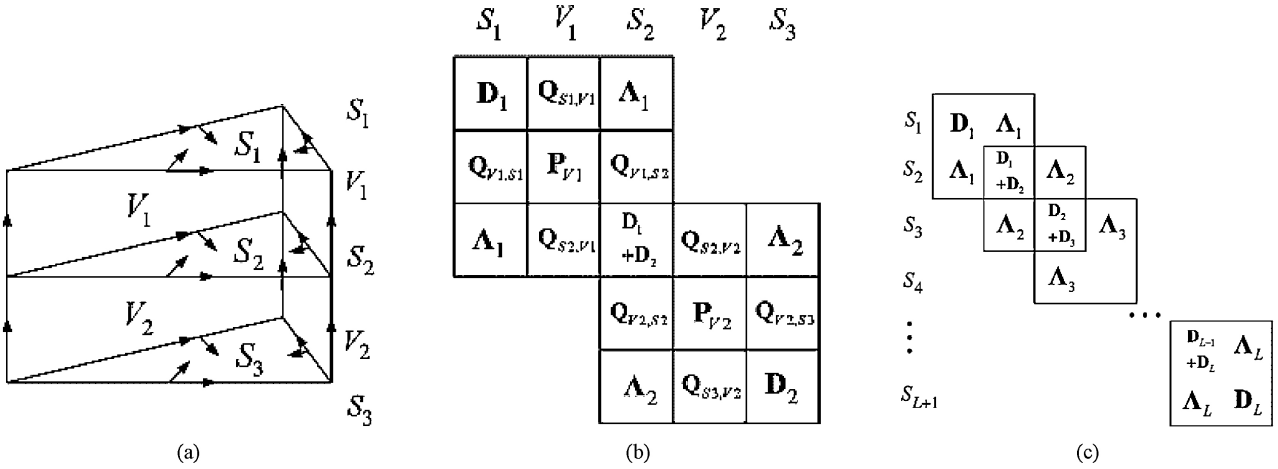

Fig. 1. (a) Prism-element discretization. (b) 3-D layered system matrix with diagonal $\mathbf{D}_i$ and Λ_i matrices. (c) 2-D layered system matrix with diagonal $\mathbf{D}_i$ and Λ_i matrices.

solution of a generalized eigenvalue problem can be converted to the solution of a matrix equation.

The algorithm of a k-step Arnoldi process for solving (6) is as follows [10]:

Algorithm: A k-step Arnoldi process

$$
\begin{aligned}
&1.\ v_1 = v_1/||v_1|| \\
&2.\ \text{for} \quad j = 1, 2, \cdots, k \quad \text{do} \\
&\quad 2.1.\ w = \mathbf{B}'^{-1}\mathbf{A}'v_j \\
&\quad 2.2.\ \text{for} \quad i = 1, 2, \cdots, j \quad \text{do} \\
&\qquad h_{ij} = v_i^* w \\
&\qquad w = w - h_{ij} v_i \\
&\quad 2.3.\ h_{j+1,i} = ||w|| \\
&\qquad v_{j+1} = w/h_{j+1,j}.
\end{aligned} \tag{7}
$$

From the above, it can be seen that the computational bottleneck of a k-step Arnoldi process is Step 2.1, the computation of $\mathbf{B}'^{-1}\mathbf{A}'v$ at each iteration step, where v is an arbitrary vector of length N. Since $\mathbf{A}'$ is sparse, $\mathbf{A}'v$ can be computed in linear complexity. As a result, the computational bottleneck becomes the computation of $\mathbf{B}'^{-1}q$, where q is a known vector. An iterative solution of $\mathbf{B}'^{-1}q$ is computationally expensive when the number of iterations is large. In addition, the number of iterations typically grows with matrix size, and hence the complexity of an iterative solution is in general higher than linear. A direct solution of $\mathbf{B}'^{-1}q$ is also computationally expensive when the matrix size N is large. The optimal complexity of directly solving a finite-element-based sparse matrix is shown to be $O(N^{1.5})$ [15]. The fast methods developed in [2] and [3] can be employed to reduce the complexity of solving $\mathbf{B}'^{-1}q$. With these methods, we can first transform matrices $\mathbf{T}$ and $\mathbf{R}$ in $\mathbf{B}'$ to block tridiagonal matrices by permuting the ordering of the underlying variables. We then reduce the system matrix, solve the reduced system by the UV parametrization method, and recover other unknowns. As a result, the computational complexity becomes $N_s O(N)$ [1]. For the problems considered in [2] and [3], N_s is the number of dielectric stacks, which is a constant for each processing technology node. However, for general 3-D problems considered in this paper, N_s is the number of unknowns on a 2-D surface, which grows with N when the problem size increases. Therefore, the complexity of the fast eigenvalue solver in [1] is also higher than linear for general 3-D problems. In the next section, we show how to solve $\mathbf{B}'^{-1}q$ in linear complexity, thus reducing the computational complexity of an Arnoldi-based generalized eigenvalue solution to $O(N)$ for general 3-D problems in ICs.

2) *Reducing the Solution of $\mathbf{B}'$ to the Solution of $\mathbf{T}$:* As can be seen from (5) and (6), $\mathbf{B}'$ consists of both $\mathbf{T}$ and $\mathbf{R}$, where $\mathbf{T}$ is a mass matrix associated with permittivity and $\mathbf{R}$ is a mass matrix associated with conductivity, as given in (3). Matrix $\mathbf{T}$ is known to be positive definite and $\mathbf{R}$ is, in general, rank deficient since conductivity does not exist everywhere in an IC. In order to solve $\mathbf{B}'^{-1}q$ in linear complexity, we derive the following formula by using the Banachiewicz inversion formula [9]:

$$
\mathbf{B}'^{-1} = \begin{bmatrix} \mathbf{R} & \mathbf{T} \\ \mathbf{T} & 0 \end{bmatrix}^{-1} = \begin{bmatrix} 0 & \mathbf{T}^{-1} \\ \mathbf{T}^{-1} & -\mathbf{T}^{-1}\mathbf{R}\mathbf{T}^{-1} \end{bmatrix}. \tag{8}
$$

As a result, the computation of $\mathbf{B}'^{-1}$ is reduced to the computation of $\mathbf{T}^{-1}$. If we are able to solve $\mathbf{T}$ in linear complexity, then the computation of $\mathbf{B}'^{-1}q$ can be performed in linear complexity.

Therefore, for arbitrary vector $\{q_1, q_2\}^T$ that appears in the Arnoldi process (7), we can compute $\mathbf{B}'^{-1}\mathbf{A}'\{q_1, q_2\}^T$ required in Step 2.1 as follows:

$$
\begin{bmatrix} 0 & \mathbf{T}^{-1} \\ \mathbf{T}^{-1} & -\mathbf{T}^{-1}\mathbf{R}\mathbf{T}^{-1} \end{bmatrix} \begin{bmatrix} -\mathbf{S} & 0 \\ 0 & \mathbf{T} \end{bmatrix} \begin{Bmatrix} q_1 \\ q_2 \end{Bmatrix} = \begin{Bmatrix} q_2 \\ -\mathbf{T}^{-1}(\mathbf{S}q_1 + \mathbf{R}q_2) \end{Bmatrix} \tag{9}
$$

which only involves one matrix solve of $\mathbf{T}$ and two sparse matrix-vector multiplications $\mathbf{S}q_1$ and $\mathbf{R}q_2$.

3) *Solving $\mathbf{T}$ in Linear Complexity:* We discretize an IC into layers of triangular prism elements shown in Fig. 1(a), resulting in N_s unknowns on each surface perpendicular to the prism axis, N_v volume unknowns in each layer, and L layers along the layer-growth direction (prism-axis direction). For the example shown in Fig. 1(a), there are two layers and

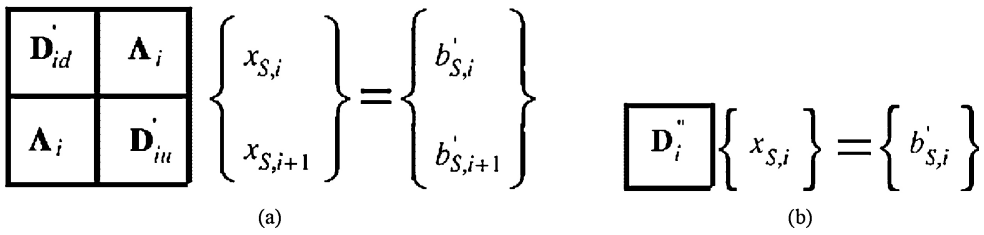

Fig. 2. (a) Single-layered system matrix. (b) Single-interface system matrix that is diagonal.

in each layer, there is one prism element. Hence, $L = 2$, $N_v = 3$, and $N_s = 6$ since there are three vector bases along the prism axis inside the volume and six vector bases on each surface in a single element. The vector bases are shown as arrows in Fig. 1(a). For more layers and more elements, the discretization shown in Fig. 1(a) extends both horizontally and vertically. The resultant matrix structure is the same block-tridiagonal structure shown in Fig. 1(b) with L diagonal blocks of size $N_s + N_v$ each. In each layer, we do not require the dielectric material to be uniform. In other words, the material can be inhomogeneous in each layer since the proposed algorithm is not restricted to layered materials. Therefore, the prism-axis direction can be aligned with any of the x, y, and z-directions in an IC. We thus can decide the layer-growth direction solely from a geometrical modeling perspective. Unknowns are ordered layer by layer as shown in Fig. 1(a). We start from surface unknowns on S_1, volume unknowns in V_1, the vector bases of which are parallel to the prism axis, surface unknowns on S_2, and continue along the prism-axis direction. By doing so, we structure the mass matrix $\mathbf{T}$ to be a 3-D layered system matrix shown in Fig. 1(b). We then further structure $\mathbf{D}_i$ and Λ_i $(i = 1, 2, \ldots, L)$ matrices in $\mathbf{T}$ to be diagonal matrices. This is achieved by employing the orthogonal prism vector basis functions developed in [4] to expand the unknown electric field $\mathbf{E}$ in each element. These orthogonal bases are complete, and also ensure tangential field continuity across the element interface. More importantly, they render the $\mathbf{D}_i$ and Λ_i blocks in $\mathbf{T}$ diagonal. In Fig. 1(b), all the $\mathbf{Q}$ matrices vanish. This is because the vector bases orientated along the prism-axis direction are perpendicular to the vector bases residing on the upper and lower surfaces of a prism element, as can be seen from Fig. 1(a). As a result, the original 3-D layered system matrix shown in Fig. 1(b) is naturally decomposed into a surface-unknown based system shown in Fig. 1(c) and L decoupled volume-unknown based subsystems $\mathbf{P}_{Vl}$ $(l = 1, 2, \ldots, L)$ without any computational cost [4].

The L-layer surface-unknown-based system shown in Fig. 1(c) can be further reduced to a single-layer surface-unknown based system shown in Fig. 2(a), where matrix $\mathbf{D}'_{id}$ carries the contribution from all the layers above layer i to layer i, while matrix $\mathbf{D}'_{iu}$ carries the contribution from all the layers below layer i to layer i. The $\mathbf{D}'_{id}$ and $\mathbf{D}'_{iu}$ can be recursively computed from the following formula:

$$\mathbf{D}'_2 = \mathbf{D}_1 + \mathbf{D}_2 - \Lambda_1 \mathbf{D}_1^{-1} \Lambda_1$$
$$\mathbf{D}'_3 = \mathbf{D}_2 + \mathbf{D}_3 - \Lambda_2 \mathbf{D}'^{-1}_2 \Lambda_2$$
$$\ldots$$
$$\mathbf{D}'_{id} = \mathbf{D}_{i-1} + \mathbf{D}_i - \Lambda_{i-1} \mathbf{D}'^{-1}_{i-1} \Lambda_{i-1}$$

and

$$\mathbf{D}'_{L-1} = \mathbf{D}_{L-1} + \mathbf{D}_L - \Lambda_L \mathbf{D}_L^{-1} \Lambda_L$$
$$\mathbf{D}'_{L-2} = \mathbf{D}_{L-2} + \mathbf{D}_{L-1} - \Lambda_{L-1} \mathbf{D}'^{-1}_{L-1} \Lambda_{L-1}$$
$$\ldots$$
$$\mathbf{D}'_{iu} = \mathbf{D}_i + \mathbf{D}_{i+1} - \Lambda_{i+1} \mathbf{D}'^{-1}_{i+1} \Lambda_{i+1}. \quad (10)$$

Since all the $\mathbf{D}_i$ and Λ_i blocks are diagonal, $\mathbf{D}'_{id}$ and $\mathbf{D}'_{iu}$ can be obtained in negligible cost. In addition, the single-layer system can be further reduced to a single-surface system as shown in Fig. 2(b), where

$$\mathbf{D}_i'' = \mathbf{D}'_{id} - \Lambda_i \mathbf{D}'^{-1}_{iu} \Lambda_i. \quad (11)$$

Again, the reduced system is diagonal, and hence can be solved readily. During the reduction process, the right-hand sides of each layer are also updated through a top-down bottom-up procedure [4]. The computational cost is also minimal because of the diagonal nature of $\mathbf{D}_i$ and Λ_i. After the surface unknowns in the reduced system are computed, the surface unknowns in other layers are recovered from

$$x_{S1,l} = \mathbf{D}'^{-1}_l [b'_{S1,l} - \Lambda_i x_{S3,l}] (l = i - 1, i - 2, \ldots, 1)$$
$$x_{S3,l} = \mathbf{D}'^{-1}_l [b'_{S3,l} - \Lambda_i x_{S3,l}] (l = i, i + 1, \ldots, L - 1)$$
$$x_{S3,l} = \mathbf{D}'^{-1}_l [b'_{S3,l} - \Lambda_i x_{S1,l}] (l = L). \quad (12)$$

It can be clearly seen that the above operations can be performed in linear complexity since only diagonal matrices $\mathbf{D}_i$ and Λ_i are involved in the procedure. The volume unknowns in each layer can be computed from $x_{Vl} = \mathbf{P}_{Vl}^{-1} b_{Vl}$ $(l = 1, 2, \ldots, L)$ in linear complexity based on the algorithm developed in [4].

B. Identification of the Spurious Eigenvalues and Its Removal

With the solution of $\mathbf{T}$ found in linear complexity, we achieved our goal of reducing the cost of a k-step Arnoldi-based solution of (6) to linear. However, there is one remaining issue that needs to be addressed. We found that the generalized eigenvalue problem (5) resulting from the orthogonal prism vector basis function-based discretization intrinsically supports a set of spurious eigenvalues. These spurious eigenvalues do not exist in a traditional prism vector basis based discretization [16]. However, they contaminate the solution of (5). In addition, the magnitude of these spurious eigenvalues is found to be similar to that of the true eigenvalues of (5). As a result, if these spurious eigenvalues are not removed, it is difficult to

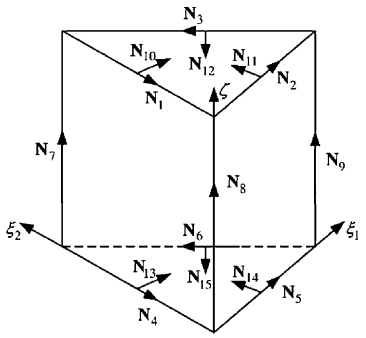

Fig. 3. Illustration of the orthogonal prism vector bases.

distinguish them from the actual eigenvalues. In this section, we explain the origin of these spurious eigenvalues and show how to remove them from the solution of (5).

In each prism element, the unknown electric field **E** is expanded by 15 orthogonal prism vector basis functions [4]. The 15 orthogonal vector bases are shown in Fig. 3 from $\mathbf{N}_1$ to $\mathbf{N}_{15}$. The degrees of freedom associated with bases $\mathbf{N}_{1-6}$ are assigned at each edge on the upper and lower surfaces that are perpendicular to the prism axis. Each of N_i (i =1-6) is purely tangential to edge i at the midpoint of the edge, thereby ensuring the tangential field continuity across the element interface. For convenience of reference, we call bases $\mathbf{N}_{10-15}$ as complementary bases in this paper. They are complementary to bases $\mathbf{N}_{1-6}$ in the sense that they supplement the normal component of the electric field at each edge on the upper and lower surfaces. Different from $\mathbf{N}_{1-6}$, the degrees of freedom of which are associated with each edge on the horizontal surfaces, and hence shared by adjacent triangular elements, $\mathbf{N}_{10-15}$ are not shared by adjacent triangular elements. If they are shared, since $\mathbf{N}_i$ is used to expand **E**, then the normal component of **E** across a material interface that separates two triangular elements will become continuous, which is wrong. As a result, the $\mathbf{N}_{10-15}$ are not shared by the prism elements that are horizontally adjacent to each other, although they are shared by the prism elements that are vertically adjacent to each other (vertical direction is along the prism axis). Therefore, in each layer, the $\mathbf{N}_{10-15}$ bases are associated with each prism element instead of each edge. In other words, there is a different set of $\mathbf{N}_{10-15}$ in each prism element. To better illustrate this point, in Fig. 4, we show a discretization that consists of four triangular prism elements. The basis functions used to discretize the four elements can be divided into two groups: the vector bases whose degrees of freedom are assigned to each edge and the complementary bases $\mathbf{N}_{10-15}$ whose degrees of freedom are assigned to each element in each layer. Therefore, there exist two complementary bases that are normal to one edge to allow for the normal continuity of the electric flux across element interfaces to be satisfied in the variational process of a finite-element procedure.

The complementary bases, being not shared by horizontally adjacent prism elements, make the eigenvalue system (5) naturally support a set of spurious eigenvalues. These eigenvalues are local resonances generated from a reduced eigenvalue system that is only formed by complementary

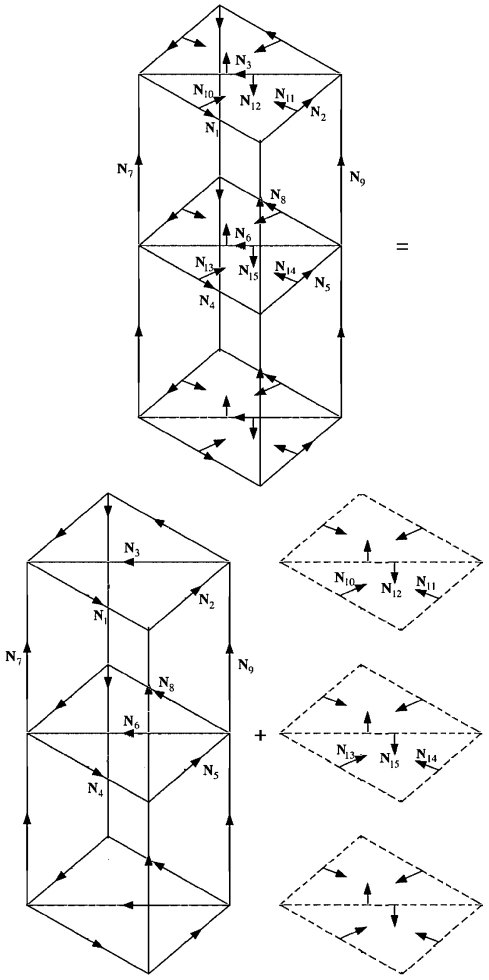

Fig. 4. Illustration of the origin of the spurious eigenvalues.

TABLE I
LOWEST EIGENVALUES k_0 (M^{-1}) OF A CAVITY

Analytical Values	Eigenvalues of the Original System	Eigenvalues of the System of Complementary Bases
	328.63 × 18 repetitions	328.63 × 18 repetitions
523.60	546.83×1	
702.50	704.54×1	
753.10	732.19×1	
	734.85 × 18 repetitions	734.85 × 18 repetitions

bases, as shown in Fig. 5(b). In this figure, C1 denotes the surface unknowns associated with the complementary bases in surface 1, C2 denotes the surface unknowns associated with the complementary bases on surface 2, etc. The solution of the complementary basis-only-based system together with the zero solutions for unknowns associated with other basis functions constitute a valid solution of the original system shown in (5). Although numerically supported by (5), the eigenvalues solved from the reduced system shown in Fig. 5(b) correspond to the local resonances of the complementary basis-only-based subsystem, and hence are not physical for the entire system.

The aforementioned theoretical analysis of the spurious eigenvalues has been verified by numerical experiments. As an example, in Table I, we list the eigenvalues of a rectangular

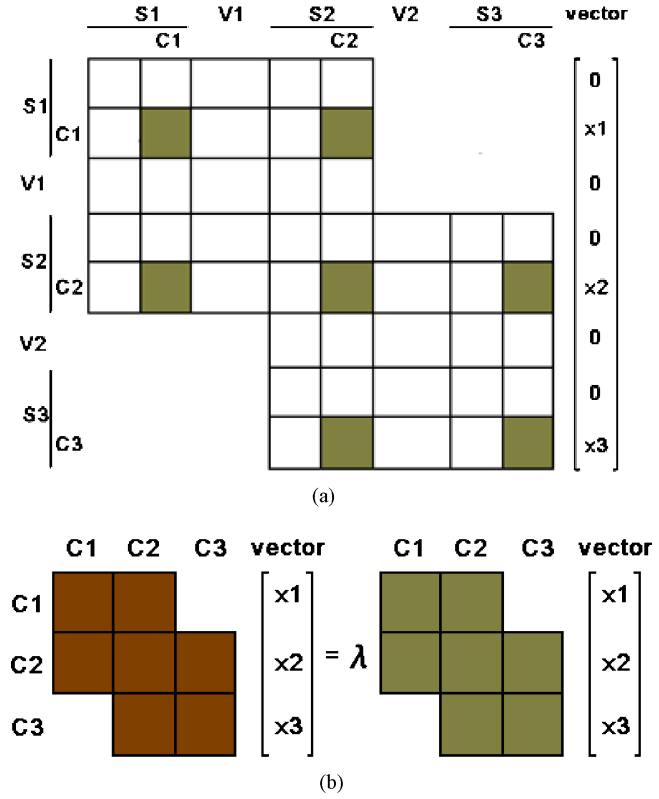

Fig. 5. (a) Original system formed by all basis functions. (b) Reduced eigenvalue problem formed by complementary bases.

cavity of size $1 \times 0.5 \times 0.75\,\text{cm}^3$ computed from the proposed orthogonal basis-based eigenvalue solver. As can be seen from Table I, in addition to the three eigenvalues that agree with analytical data, two spurious eigenvalues are also generated, each of which is repeated for 18 times. These two spurious eigenvalues are exactly the same as those solved from the reduced eigenvalue system that only consists of complementary bases shown in Fig. 5(b).

With the origin of the spurious eigenvalues identified, it becomes obvious how to remove these unwanted eigenvalues. If the entries corresponding to noncomplementary bases of an eigenvector are zero, the corresponding eigenvalue (mode) is a spurious value, and hence removed. Assume that *val* is the average magnitude of the whole entries of an eigenvector, and val_{nc} is the average magnitude of the entries that correspond to the noncomplementary bases. Numerically, we can apply the following condition to remove the spurious values:

$$\frac{val_{nc}}{val} < \epsilon_{\text{err}}.$$

In the simulation conducted in this paper, the tolerance ϵ_{err} was chosen as 10^{-5}.

C. Optimally Scaled Quadratic Eigenvalue Problem

In this paper, the quadratic eigenvalue problem (2) is converted to a linear problem (5) of twice the dimension. It is shown in [14] that for the sake of accuracy, it is very important to scale the coefficient matrices **S**, **T**, and **R** before numerically computing the eigenvalues via linearization.

The backward error [13], [14] is a good measurement of the accuracy of a quadratic eigenvalue problem (4), which is defined as

$$\eta_P(x,\lambda) = \frac{\|(\lambda^2\mathbf{T} + \lambda\mathbf{R} + \mathbf{S})x\|_2}{(|\lambda|^2\|\mathbf{T}\|_2 + |\lambda|\|\mathbf{R}\|_2 + \|\mathbf{S}\|_2)\|x\|_2}. \tag{13}$$

If the matrix norm $||\mathbf{T}||_2$, $||\mathbf{S}||_2$, and $||\mathbf{R}||_2$ differ a lot in the order of magnitude, the eigenvalue algorithm applied to the linearized problem (5) may yield very poor backward errors [13]. For the physical problems considered in this paper, due to nonideal conductors and small physical dimensions at the micrometer and nanometer level, the entries of **S**, **T**, and **R** do differ from each other by orders of magnitude. As a result, we have to scale these matrices before solving the quadratic eigenvalue problem (2) for achieving good accuracy.

We employ an optimal scaling technique [13] to reduce the backward error. There are two scaling coefficients α and β involved in this technique. They are determined as the following:

$$\begin{aligned}
&\mathbf{P}(\lambda) = \lambda^2\mathbf{T} + \lambda\mathbf{R} + \mathbf{S}\\
&\gamma_2 = ||\mathbf{T}||_2, \quad \gamma_1 = ||\mathbf{R}||_2, \quad \gamma_0 = ||\mathbf{S}||_2\\
&\alpha = \sqrt{\gamma_0/\gamma_2}\\
&\beta = 2/(\gamma_0 + \gamma_1\sqrt{\gamma_0/\gamma_2}).
\end{aligned}$$

Based on the optimal scaling coefficients, we convert the original quadratic problem **P** shown in (4) to a scaled quadratic problem $\mathbf{P}'$ as follows:

$$\mathbf{P}' = \mathbf{P}(\lambda)\beta = \lambda'^2(\mathbf{T}\alpha^2\beta) + \lambda'(\mathbf{R}\alpha\beta) + (\mathbf{S}\beta)$$

where $\lambda = \lambda'\alpha$. As a result, the scaled quadratic eigenvalue problem becomes

$$[\mathbf{S}'' + \lambda'^2\mathbf{T}'' + \lambda'\mathbf{R}'']\{e\} = 0, \qquad (\lambda' = \lambda/\alpha) \qquad (2')$$

in which $\mathbf{S}''=\beta\mathbf{S}$, $\mathbf{T}''=\alpha^2\beta\mathbf{T}$, and $\mathbf{R}''=\alpha\beta\mathbf{R}$. Here, the eigenvector e remains the same as that in the original quadratic eigenvalue problem. Since this method is very effective in balancing the scales of the coefficient matrices in (2), we can significantly reduce the backward error of **P** and improve the accuracy of the proposed eigenvalue solution. After solving $(2')$ with respect to λ', λ can be obtained by multiplying λ' by α. The effectiveness of this algorithm will be validated in the following section.

IV. Numerical Results

We simulate a number of examples to demonstrate the accuracy and linear complexity of the proposed eigenvalue solver.

A. Half-Filled Cavity

The proposed linear-complexity eigenvalue solver is first validated with a lossy cavity structure that has an analytical solution. The cavity is filled with a conductive material as shown in Fig. 6, and shielded by electric walls. Two methods are compared. One is the proposed orthogonal eigenvalue solver. The other is the UV-RR-based solver developed in [1]. The number of unknowns generated by the proposed method is 1792. The number of unknowns resulting from a

TABLE II
LOWEST RESONANT FREQUENCIES AND CPU TIME COST OF A HALF-FILLED CAVITY

σ (S/m)	Analytical Values [6]	UV-RR Solver [1] N = 1926			Proposed Orthogonal Solver N = 1792		
	f_r (GHz)	f_r (GHz)	Error (%)	Time (ms)	f_r (GHz)	Error (%)	Time (ms)
1.3	5.711 + j5.197	5.808 + j5.154	1.37	68.71	5.652 + j5.244	0.98	9.35
1.0	6.579 + j3.864	6.645 + j3.831	0.97	69.23	6.545 + j3.897	0.62	9.40
0.5	7.236 + j1.819	7.282 + j1.805	0.64	74.99	7.222 + j1.833	0.27	9.31
0.1	7.379 + j0.354	7.423 + j0.352	0.59	68.56	7.368 + j0.357	0.16	9.39

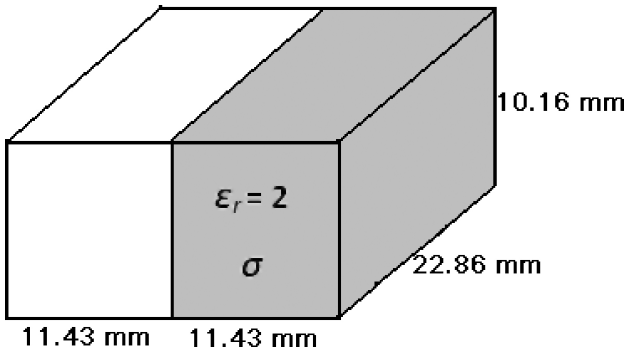

Fig. 6. Half-filled cavity structure.

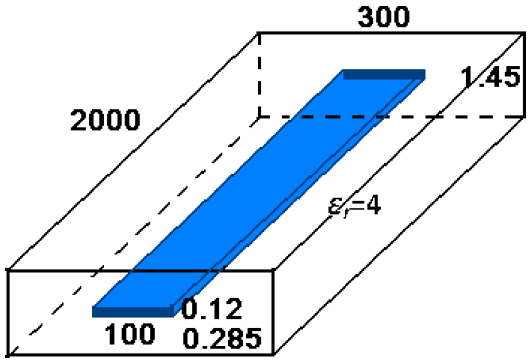

Fig. 7. Illustration of an on-chip single stripline-type interconnect (geometrical unit: μm).

traditional prism vector basis-based discretization used in the UV-RR method is 1926. The Heisenberg size computed in the Arnoldi iteration is 500 for both methods. In Table II, we list the resonant frequencies f obtained by the proposed solver and those computed by the UV-RR-based solver in comparison with analytical data $f_{\text{analytical}}$. The error is assessed by $|f_{\text{analytical}} - f|/|f_{\text{analytical}}|$. Very good accuracy is observed from the proposed solver. In addition, compared to the UV-RR solver, the CPU time cost by the proposed orthogonal eigenvalue solver is significantly smaller. The unit of CPU time is millisecond in Table II.

B. On-Chip Single Stripline-Type Interconnect

The second example is an on-chip interconnect that is a single stripline-type structure. As shown in Fig. 7, the structure is filled with a dielectric material of relative permittivity 4, and shielded by perfect electric conductors on the top and at the bottom. The other four boundaries are left open (Neumann-type boundary conditions). The structure is of size $1.45 \times 300 \times 2000\,\mu\text{m}^3$. A copper strip, with conductivity 5×10^7 S/m and thickness $0.12\,\mu$m, is located in the center of the structure. The size of the system matrix $\mathbf{A}'$ and $\mathbf{B}'$ is 4193. The Heisenberg matrix size (the number of Arnoldi iterations performed) is 1000.

TABLE III
LOWEST FIVE RESONANT FREQUENCIES (GHZ) OF AN ON-CHIP SINGLE STRIPLINE INTERCONNECT

MATLAB (N = 4145)	UV-RR Solver [1] (N = 4145)	Proposed Solver (N = 3927)
47.5 + j51.6	47.48 + j51.58	47.47 + j51.57
97.7 + j54.2	97.73 + j54.20	97.71 + j54.20
149.0 + j57.7	149.04 + j57.70	149.00 + j57.72
198.0 + j61.0	198.03 + j60.99	197.98 + j61.04
220.8 + j62.4	220.83 + j62.36	220.78 + j62.43

In Table III, we list the five lowest resonant frequencies computed from the proposed eigenvalue solver, which are sorted by real part. They show excellent agreement with the eigenvalues obtained from MATLAB and those computed by the UV-RR solver [1].

With this structure, we also examine the performance of the optimal scaling method described in Section III-C. The backward error obtained by the optimal scaling with $\alpha = 8.8 \times 10^7$ and $\beta = 0.08$ is shown to be, in general, smaller than that generated by a simple scaling with scaling coefficients $\alpha = 10^7$ and $\beta = 1$, as can be seen from Table IV. From Table V, it can also be seen clearly that the zero eigenvalues of (5) are computed more accurately by the scaling techniques. Both simple scaling and optimal scaling produce more accurate zeros compared to the eigenvalue solution without any scaling. The simple scaling, though not optimal, is also an effective scaling technique. It is developed based on the goal of balancing the scale of matrices $\mathbf{S}$, $\mathbf{T}$, and $\mathbf{R}$ in (2). As can be seen from (3), the major difference between the scale of $\mathbf{R}$ and that of $\mathbf{T}$ is conductivity σ. Thus, we use the magnitude of metal conductivity, which is at the level of 10^7, to scale $\mathbf{T}$ and $\mathbf{R}$. By doing so, the scaled matrix $\mathbf{T}''=\alpha^2\mathbf{T}$ becomes close to $\mathbf{R}''=\alpha\mathbf{R}$ in magnitude. Moreover, they both become close to matrix $\mathbf{S}$ in magnitude.

C. On-Chip Power Grid Structure

The third example is an on-chip power grid structure as shown in Fig. 8. There are two x-direction wires, four y-direction wires, and four vias that connect the crossing wires of the same polarity. The structure is shielded by a perfect electric conducting plane on the top and at the bottom, with the other four sides left open. The conductivity of all wires is 5×10^7 S/m.

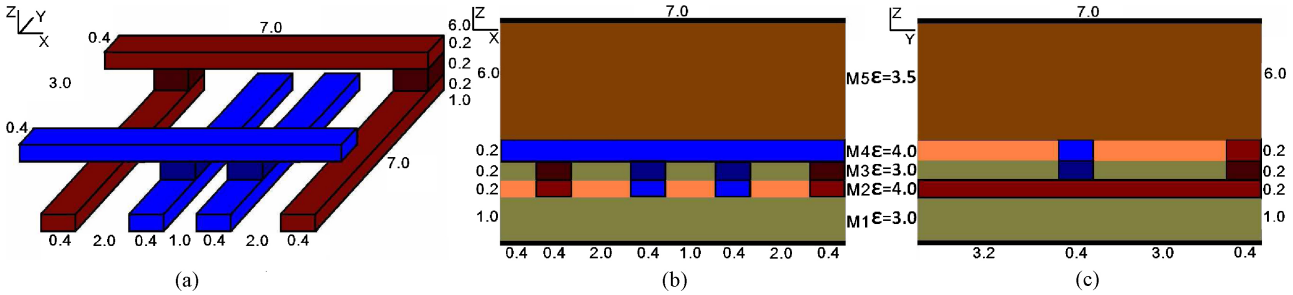

Fig. 8. Illustration of an on-chip power grid structure (geometrical unit: μm). (a) 3-D view. (b) xz-plane view. (c) yz-plane view.

TABLE IV
BACKWARD ERRORS OF AN ON-CHIP SINGLE STRIPLINE INTERCONNECT

Resonant Frequency	Backward Error with Simple Scaling	Backward Error with Optimal Scaling
47.5 + j51.6	2.72×10^{-6}	3.97×10^{-7}
97.7 + j54.2	8.40×10^{-6}	7.82×10^{-7}
149.0 + j57.7	5.96×10^{-6}	2.23×10^{-6}
198.0 + j61.0	1.72×10^{-5}	3.37×10^{-5}
220.8 + j62.4	1.30×10^{-5}	8.87×10^{-6}

TABLE V
COMPARISON OF THE COMPUTED EIGENVALUES (GHZ) WITH AND WITHOUT SCALING

Eigenvalues Computed Without Scaling	Eigenvalues Computed with Simple Scaling	Eigenvalues Computed with Optimal Scaling
2.5 + j22629.6	0.0041 + j0.0009	0.0007 − j0.0001
5.9 + j22584.1	0.0044 + j0.0000	0.0007 − j0.0001
3.2 + j22628.9	0.0053 − j0.0043	0.0012 − j0.0019
46.9 + j51.5	47.5 + j51.6	47.5 + j51.6
92.3 + j54.6	97.7 + j54.2	97.7 + j54.2
138.3 + j97.4	149.0 + j57.7	149.0 + j57.7

TABLE VI
LOWEST FOUR RESONANT FREQUENCIES OF AN ON-CHIP POWER GRID STRUCTURE (UNIT: GHZ)

MATLAB $N = 4452$	Proposed Solver $N = 4452$
3811.658286 + j117.423338	3811.658286 + j117.423337
6030.105281 + j142.290841	6030.105281 + j142.290842
7809.571017 + j174.781751	7809.571007 + j174.781749
8538.366505 + j27.122742	8538.366505 + j27.122742

In Table VII, we list the lowest four eigenvalues generated by the proposed solver. The backward error obtained by solving the scaled eigenvalue problem and that obtained by solving the original eigenvalue problem are also compared in this table. The scaling coefficients are $\alpha = 3.51 \times 10^6$ and $\beta = 549$. Clearly, the accuracy of the eigenvalue solution is improved by a few orders of magnitude owing to the optimal scaling technique. When assessing the backward error shown in (13), both eigenvectors and eigenvalues are used in the calculation. Therefore, the accuracy of both eigenvalues and eigenvectors of the proposed solver is validated.

We also compare the eigenvalues generated from the proposed solver with those generated by MATLAB in Table VI. Excellent agreement is observed.

TABLE VII
BACKWARD ERRORS OF A POWER GRID STRUCTURE

Eigenvalues	Backward Error Without Scaling	Backward Error With Scaling
3811.66 + j117.42	3.43×10^{-4}	1.65×10^{-7}
6030.11 + j142.29	2.28×10^{-4}	1.68×10^{-7}
7809.57 + j174.78	3.94×10^{-6}	6.98×10^{-8}
8538.37 + j27.12	3.95×10^{-6}	7.35×10^{-8}

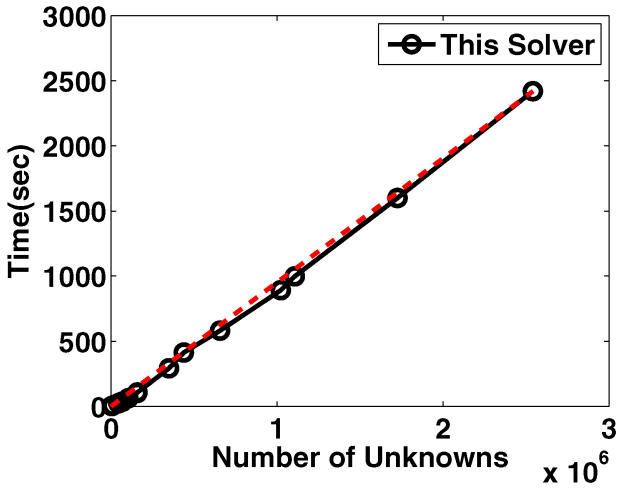

Fig. 9. Arnoldi time versus the number of unknowns.

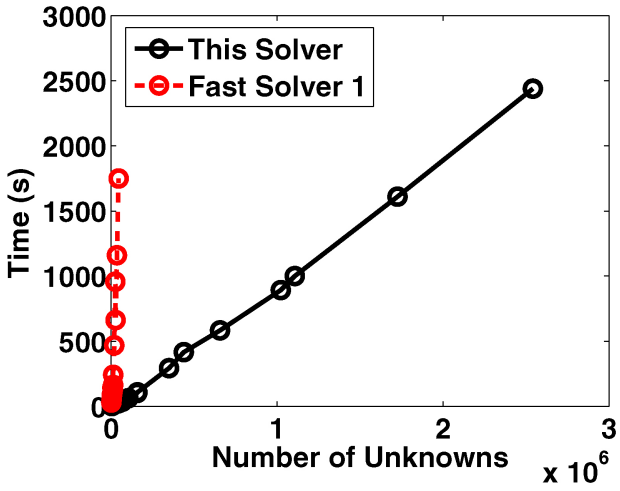

Fig. 10. Total CPU time cost versus the number of unknowns.

TABLE VIII
ARNOLDI TIME VERSUS THE NUMBER OF UNKNOWNS

UV-RR Solver ([1])		Proposed Solver		MATALB
N	CPU Time (s)	N	CPU Time (s)	CPU Time (s)
1492	28	1536	0.77	163
2968	46	3584	1.80	154
7626	128	7854	3.87	185
9792	137	9312	4.94	1960
18 954	369	17 708	9.95	3570

TABLE IX
BREAKDOWN OF THE TOTAL CPU TIME OF THE PROPOSED SOLVER

N	Decomposition Time (s)	Arnoldi Time (s)	QR Time (s)	Total Time (s)
1536	1.821×10^{-4}	0.77	4.072×10^{-2}	0.811
3584	5.161×10^{-4}	1.80	6.779×10^{-2}	1.868
7854	1.305×10^{-4}	3.87	7.589×10^{-2}	3.946
9312	1.629×10^{-4}	4.94	6.765×10^{-2}	5.009
17 708	5.691×10^{-4}	9.95	4.226×10^{-2}	10

In addition to the accuracy analysis, we assess the efficiency of the proposed method. In Table VIII, we compare the Arnoldi iteration time cost by the proposed solver with that cost by the UV-RR solver, and that by the eigensolver of MATLAB, respectively. The number of Arnoldi iterations performed is 1000. The examples simulated are a series of power grids obtained by varying the size of the power grid shown in Fig. 8. The size is increased by duplicating the power grid shown in Fig. 8 along x direction multiple times with the discretization density kept the same, and the prism axis (layer growth direction) along y. It is clear that the proposed solver is orders of magnitude faster than both of the UV-RR solver and MATLAB that employs a state-of-the-art sparse-matrix-based eigenvalue solver. The total CPU time of the proposed solver includes the time cost in reduction and decomposition of the reduced single-layer matrices in $\mathbf{T}$ before the Arnoldi iteration, the Arnoldi iteration, and the QR process after Arnoldi iteration. The cost in each step is listed in Table IX. The recovery time is included in the Arnoldi iteration time because the unknowns in each layer need to be recovered to construct a complete vector at each Arnoldi step. The decomposition time is negligible because the reduction is based on diagonal matrices and the reduced single-layer matrices are either diagonal or tridiagonal in the orthogonal finite-element reduction recovery-based solution of matrix $\mathbf{T}$.

Moreover, we validate the computational complexity of the proposed eigenvalue solver. We plot the Arnoldi iteration time with respect to N in Fig. 9, in which the dashed line represents the CPU time that scales with N linearly. The linear complexity of the proposed solver is clearly demonstrated. In Fig. 10, the total CPU time for the proposed eigenvalue solver is plotted with respect to N in comparison with the UV-RR solver developed in [1]. It is clear that the proposed solver has a linear complexity whereas the UV-RR solver does not. This is because the complexity of the UV-RR solver is $O(N_s N)$. When the number of unknowns on a single surface N_s also increases with N, the complexity of the UV-RR solver is higher than $O(N)$. As can be seen from Fig. 9, the quadratic

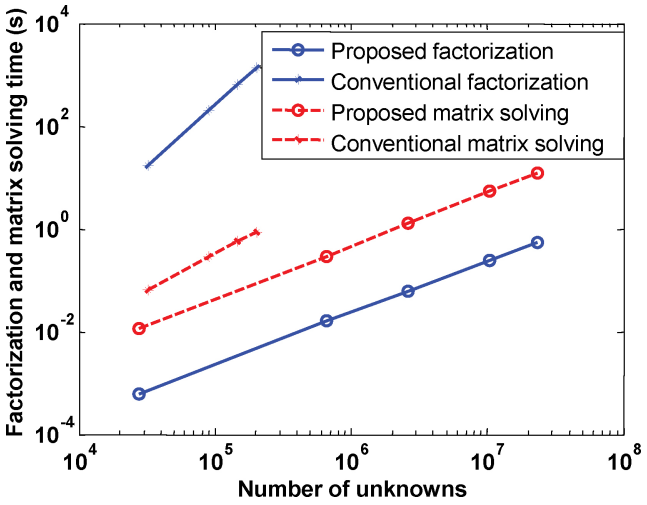

Fig. 11. Matrix factorization and solution time in the proposed eigenvalue solution in comparison with that in a conventional solver.

TABLE X
LOWEST EIGHT RESONANT FREQUENCIES OF A PACKAGE SPIRAL INDUCTOR (UNIT: GHZ)

Proposed Solver	UV-RR Solver
38.059 + j0.002	38.297 + j0.002
80.159 + j0.003	80.576 + j0.003
119.354 + j0.001	119.773 + j0.001
135.415 + j0.001	135.644 + j0.001
154.899 + j0.002	155.592 + j0.001
173.059 + j0.001	173.435 + j0.001
202.005 + j0.002	203.443 + j0.002
235.163 + j0.002	236.271 + j0.002

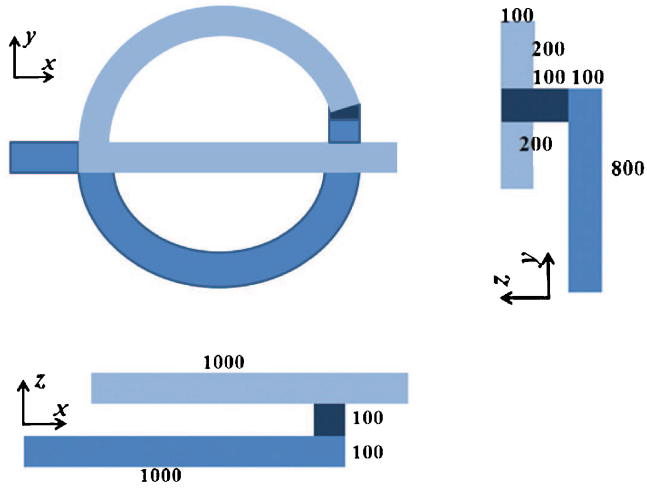

Fig. 12. Illustration of a two-metal-layer package spiral inductor structure (geometrical unit: μm).

eigenvalue problem involving over 2.5 million unknowns is solved in 40 min. The computer used has a single 8222SE AMD Opteron processor running at 3 GHz.

Furthermore, we considered a realistic on-chip power grid provided by Intel Corporation. The structure involved M4, M5, M6, and M7 metal layers. In between, there are a large number of vias connecting orthogonal power rails at different metal layers. We simulated a suite of such power

grid examples, which occupy a chip area from 11.43×12.86, 57.15×64.3, 114.3×128.6, and 228.6×257.2, to $342.9 \times 385.8\,\mu\text{m}^2$, resulting in 27 742, 658 870, 2 618 230, 10 438 450, and 23 460 670 unknowns, respectively. Since the cost of the proposed eigenvalue solution at each Arnoldi step is the solution of $\mathbf{T}$ as shown in (9), in Fig. 11, we plotted the time for factorizing $\mathbf{T}$ and solving $\mathbf{T}$ versus the number of unknowns in the proposed solution in comparison with the conventional solver that employs a state-of-the-art multifrontal-based sparse matrix solver (UMFPACK5.0 at http://www.cise.ufl.edu/research/sparse/umfpack/). Clearly, in the proposed eigenvalue solution, $\mathbf{T}$ is factorized and solved in linear complexity. The matrix factorization time is even less than the matrix solving time because of matrix blocks that are diagonalized by the orthogonal vector bases. The CPU cost of the conventional solver was not plotted across the entire unknown range because it failed to solve a larger number of unknowns due to large memory requirements.

D. Package Spiral Inductor

To demonstrate the capability of the proposed method in solving irregularly shaped 3-D structures, we simulated a package spiral inductor shown in Fig. 12. The layout of the spiral inductor occupied two metal layers, with the dark-colored half ring residing on the lower metal layer and the light-colored one located on the top metal layer. The two half rings were connected by a vertical via, which is shown by the darkest block in Fig. 12. The metal conductivity is 5×10^7 S/m. There are five layers. The thickness of each layer is $100\,\mu$m. The dielectric constant is 1 in each layer. The computational domain was truncated by a perfect electric conducting boundary condition on the top, at the bottom, and at the leftmost and rightmost boundaries. The other two ends (yz-planes) were left open. The geometrical parameters in μm unit of the spiral inductor are given in Fig. 12. The discretization of the structure resulted in 14 091 unknowns. The number of Arnoldi iterations performed was 3000. The smallest eight resonant frequencies extracted by the proposed eigenvalue solver are listed in Table X in comparison with those generated by the UV-RR solver developed in [1]. Excellent agreement can be observed.

V. Conclusion

In this paper, a 3-D complex-valued quadratic eigenvalue solver of linear complexity was developed for electromagnetics-based analysis of large-scale ICs. The linear complexity was achieved with a new quadratic eigenvalue formulation and a linear-complexity solution of the large-scale sparse matrix involved in the Arnoldi iteration. Furthermore, we identified the spurious eigenvalues that were intrinsically supported by an orthogonal prism element-based discretization of the quadratic eigenvalue problem. We analyzed the origin of these eigenvalues and showed how to remove them effectively. In addition, we introduced the backward error to measure the accuracy of a quadratic eigenvalue solution, and employed an optimal scaling technique to transform the original quadratic eigenvalue problem to a scaled quadratic eigenvalue problem, which improved the accuracy of the quadratic eigenvalue solution by a few orders of magnitude. Numerical results have demonstrated the accuracy and efficiency of the proposed method. In addition to predicting the global resonances of IC systems, the proposed method can be employed to perform a modal analysis of general 3-D electromagnetic structures.

References

[1] J. Lee, V. Balakrishnan, C.-K. Koh, and D. Jiao, "A fast 3-D eigenvalue solver for finite-element-based analysis of multilayered integrated circuits," in *Proc. IEEE Int. Symp. AP-S*, Jul. 2010, pp. 1–4.

[2] J. Lee, V. Balakrishnan, C.-K. Koh, and D. Jiao, "A linear-time complex-valued eigenvalue solver for electromagnetic analysis of large-scale on-chip interconnect structures," *IEEE Trans. Microwave Theory Tech.*, vol. 57, no. 8, pp. 2021–2029, Aug. 2009.

[3] J. Lee, V. Balakrishnan, C.-K. Koh, and D. Jiao, "From $O(k^2N)$ to $O(N)$: A fast complex-valued eigenvalue solver for large-scale on-chip interconnect analysis," *IEEE Trans. Microwave Theory Tech.*, vol. 57, no. 12, pp. 3219–3228, Dec. 2009.

[4] D. Chen and D. Jiao, "Time-domain orthogonal finite-element reduction-recovery (OrFE-RR) method for electromagnetics-based analysis of large-scale integrated circuit and package problems," *IEEE Trans. Comput. Aided Des. Integr. Circuits Syst.*, vol. 28, no. 8, pp. 1138–1149, Aug. 2009.

[5] R. Lehoucq, K. Maschhoff, D. Sorensen, and C. Yang. *ARPACK Software* [Online]. Available: http://www.caam.rice.edu/software/ARPACK

[6] J. Lee, T. Xiao, and Q. H. Liu, "A 3-D spectral-element method using mixed-order curl conforming vector basis functions for electromagnetic fields," *IEEE Trans. Microwave Theory Tech.*, vol. 54, no. 1, pp. 437–444, Jan. 2006.

[7] J. Jin, *The Finite Element Method in Electromagnetics*. New York: Wiley, 2002.

[8] D. Jiao, M. Mazumder, S. Chakravarty, C. Dai, M. Kobrinsky, M. Harmes, and S. List, "A novel technique for full-wave modeling of large-scale three-dimensional high-speed on/off-chip interconnect structures," in *Proc. Int. Conf. SISPAD*, Sep. 2003, pp. 39–42.

[9] F. Zhang, *The Schur Complement and Its Applications*. New York: Springer, 2003.

[10] D. B. I. Lloyd and N. Trefthen, *Numerical Linear Algebra*. Philadelphia, PA: SIAM, 1997.

[11] B. N. Parlett and C. Reinsch, "Balancing a matrix for calculation of eigenvalues and eigenvectors," *Numeric. Math.*, vol. 13, no. 4, pp. 293–304, Aug. 1969.

[12] R. A. Horn and C. R. Johnson, *Topics in Matrix Analysis*. Cambridge, U.K.: Cambridge Univ. Press, 1991.

[13] H.-Y. Fan, W.-W. Lin, and P. Van Dooren, "Normwise scaling of second order polynomial matrices," *SIAM J. Matrix Anal. Applicat.*, vol. 26, no. 1, pp. 252–256, Sep. 2004.

[14] N. J. Higham, D. S. Mackey, F. Tisseur, and S. D. Garvey, "Scaling, sensitivity and stability in the numerical solution of quadratic eigenvalue problems," *Int. J. Numeric. Methods Eng.*, vol. 73, no. 3, pp. 344–360, Jan. 2008.

[15] A. George, "Nested dissection of a regular finite element mesh," *SIAM J. Numeric. Anal.*, vol. 10, no. 2, pp. 345–363, Apr. 1973.

[16] R. D. Graglia, D. R. Wilton, A. F. Peterson, and I. Gheorma, "Higher order interpolatory vector bases on prism elements," *IEEE Trans. Antennas Propag.*, vol. 46, no. 3, pp. 442–450, Mar. 1998.

Jongwon Lee (S'09) received the B.S. degree in electrical engineering from Seoul National University, Seoul, Korea, in 2002, and the M.S. and Ph.D. degrees in electrical and computer engineering from Purdue University, West Lafayette, IN, in 2007 and 2010, respectively.

From 2002 to 2005, he was a System Programmer with Chosun-Ilbo, Seoul, Korea. In January 2011, he joined the Agency for Defense Development, Daejeon, Korea, where he is currently a Senior Researcher. His current research interests include computational electromagnetics for circuit design and the analysis of high-power microwave systems.

Duo Chen received the B.S. and M.S. degrees in electrical engineering from Tsinghua University, Beijing, China, in 2004 and 2007, respectively. He is currently pursuing the Ph.D. degree from the School of Electrical and Computer Engineering, Purdue University, West Lafayette, IN.

He is a Research Assistant with the On-Chip Electromagnetics Research Group, School of Electrical and Computer Engineering, Purdue University. His current research interests include electromagnetics-based analysis of very large-scale integrated problems.

Venkataramanan Balakrishnan (M'94–SM'06) received the B.Tech. degree in electronics and communication from the Indian Institute of Technology, Madras, India, in 1985, the M.S. degree in statistics from Stanford University, Palo Alto, CA, and the Ph.D. degree in electrical engineering in 1992.

Since 1994, he has been with the Faculty of Electrical and Computer Engineering at Purdue University, West Lafayette, IN, where he is currently a Professor and Head. His current research interests include applying numerical techniques, especially those based on convex optimization, to problems in engineering. He is a coauthor of the monograph *Linear Matrix Inequalities in System and Control Theory* (Philadelphia, PA: SIAM, 1994).

Dr. Balakrishnan received the President of India Gold Medal from the Indian Institute of Technology, in 1985, the Young Investigator Award from the Office of Naval Research in 1997, the Ruth and Joel Spira Outstanding Teacher Award in 1998, and the Honeywell Award for Excellence in Teaching in 2001 from the School of Electrical and Computer Engineering at Purdue University. He was named a Purdue University Faculty Scholar in 2008.

Cheng-Kok Koh (S'92–M'98–SM'06) received the B.S. (with first class honors) and M.S. degrees in computer science from the National University of Singapore, Singapore, in 1992 and 1996, respectively, and the Ph.D. degree in computer science from the University of California at Los Angeles (UCLA), Los Angeles, in 1998.

He is currently a Professor of electrical and computer engineering with Purdue University, West Lafayette, IN. His current research interests include physical design of very large-scale integrated circuits and modeling and analysis of large-scale systems.

Dr. Koh was the recipient of the 1990 Lim Soo Peng Book Prize for Best Computer Science Student presented by the National University of Singapore, the Tan Kah Kee Foundation Postgraduate Scholarship in 1993 and 1994, the GTE Fellowship and the Chorafas Foundation Prize presented by UCLA, in 1995 and 1996, the 1998 ACM Special Interest Group on Design Automation Meritorious Service Award and Distinguished Service Award, the 1999 Chicago Alumni Award presented by Purdue University, the 2000 National Science Foundation CAREER Award, and the 2002 ACM/SIGDA Distinguished Service Award.

Dan Jiao (S'00–M'02–SM'06) received the Ph.D. degree in electrical engineering from the University of Illinois at Urbana-Champaign, Urbana, in 2001.

She then joined the Technology Computer-Aided Design (CAD) Division, Intel Corporation, Santa Clara, CA, until September 2005, as a Senior CAD Engineer, Staff Engineer, and a Senior Staff Engineer. In September 2005, she joined Purdue University, West Lafayette, IN, as an Assistant Professor with the School of Electrical and Computer Engineering, where she is currently a tenured Associate Professor. She has authored two book chapters and over 140 papers in refereed journals and international conferences. Her current research interests include computational electromagnetics, high-frequency digital, analog, mixed-signal, and radio frequency (RF) integrated circuit design and analysis, high-performance very large-scale integrated CAD, modeling of microscale and nanoscale circuits, applied electromagnetics, fast and high-capacity numerical methods, fast time-domain analysis, scattering and antenna analysis, RF, microwave, and millimeter-wave circuits, wireless communication, and bio-electromagnetics.

Dr. Jiao has served as the reviewer for many IEEE journals and conferences. She was among the 100 engineers selected for the National Academy of Engineering's 2011 U.S. Frontiers of Engineering Symposium. She was the 2010 recipient of the Ruth and Joel Spira Outstanding Teaching Award, the 2008 National Science Foundation CAREER Award, the 2006 Jack and Cathie Kozik Faculty Start up Award (which recognizes an outstanding new Faculty Member of the School of Electrical and Computer Engineering, Purdue University), the 2006 Office of Naval Research Award under the Young Investigator Program, the 2004 Best Paper Award presented at the Intel Corporation's Annual Corporate-Wide Technology Conference (Design and Test Technology Conference) for her work on generic broadband model of high-speed circuits, the 2003 Intel Corporation's Logic Technology Development (LTD) Divisional Achievement Award in recognition of her work on the industry-leading BroadSpice modeling/simulation capability for designing high-speed microprocessors, packages, and circuit boards, the Intel Corporation's Technology CAD Divisional Achievement Award for the development of innovative full-wave solvers for high frequency IC design, the 2002 Intel Corporation's Components Research the Intel Hero Award (Intel-wide she was the tenth recipient) for the timely and accurate 2-D and 3-D full-wave simulations, the Intel Corporation's LTD Team Quality Award for her outstanding contribution to the development of the measurement capability and simulation tools for high frequency on-chip crosstalk, and the 2000 Raj Mittra Outstanding Research Award presented by the University of Illinois at Urbana-Champaign.